PHYSICAL REVIEW B **79**, 121401(R) (2009)

Micrometer-scale band mapping of single silver islands in real and reciprocal space

Y. Fujikawa,[1] T. Sakurai,[1] and R. M. Tromp[2]
[1]*Institute for Materials Research, Tohoku University, Sendai 980-8577, Japan*
[2]*IBM Research Division, T. J. Watson Research Center, 1101 Kitchawan Road, P.O. Box 218, Yorktown Heights, New York 10598, USA*
(Received 29 October 2008; revised manuscript received 20 January 2009; published 12 March 2009)

Although ultraviolet photoelectron emission spectroscopy and microscopy have served as powerful tools for electronic structure analysis in both reciprocal and real space, the integration of spectroscopy into microscopy still remains a challenge due to the technical difficulty of achieving both high spatial and energy resolution with slow electrons. We demonstrate photoelectron emission spectroscopy and microscopy covering the real, reciprocal, and energy spaces efficiently, enabled by a recently developed energy-filtered microscope. Observation of photoemission from micron-sized silver islands using He I radiation reveals the importance of the unreduced final-state wave vectors, which determine the photoelectron angular distribution.

DOI: 10.1103/PhysRevB.79.121401 PACS number(s): 79.60.Bm, 68.37.Xy, 71.20.−b, 73.20.At

Photoelectron emission has served as a fundamental probe to analyze the electronic and chemical states of materials based on the fact that quantum information is well preserved in the photoelectrons. While core-level emission by x-ray excitation has been widely used for elemental and chemical analysis, ultraviolet photoelectron spectroscopy has been applied extensively for studies of electronic valence states to understand the origin of the properties of the materials. Angle-resolved ultraviolet photoemission spectroscopy (ARUPS) measurements, accessing the electronic density of states (DOS) in energy and in two-dimensional (2D) reciprocal space, are essential for the determination of surface and bulk valence-band structure.[1]

On the other hand, recent progress in photoelectron emission microscopy (PEEM)[2] has enabled nanoscale imaging of photoelectron distribution in real space, complementing ARUPS. Observations of organic thin-film growth with low irradiation damage[3] and of plasmon wave propagation with two-photon excitation[4,5] have been achieved using PEEM, demonstrating its potential for investigations of both structural and electronic properties on the nanoscale. Combining spectroscopy with microscopy (spectromicroscopy) is a powerful experimental method to provide an even more comprehensive level of understanding. For instance, core levels have successfully been used to image chemical[6,7] and magnetic[8] domain structures, using synchrotron radiation as an excitation source.

Here, we report efficient spectromicroscopy experiments on photoelectrons excited from Ag islands on Si(111), using a conventional He I light source in conjunction with a recently developed energy-filtered low energy electron microscope (LEEM).[9] Both energy-filtered imaging and area-selected spectroscopy on Ag(111)/Ag(001) islands are demonstrated, yielding full photoelectron distribution in energy, 2D real, and 2D reciprocal space. Area-selected photoemission spectra from Ag(111) and Ag(001) areas reveal that the unreduced wave vector of the excited electron in the final state determines the strongest resonance condition of the *d*-band photoemission because of negligible scattering at the surface.

All experiments were carried out in the IBM LEEM II system[10] with an energy filter[9] as shown in Fig. 1(a). The filter entrance slit position can be precisely controlled by a motor-driven micrometer and scanned across the full electron angular distribution in the back focal plane of the objective lens. By obtaining an *E-k* spectrum for each slit position,

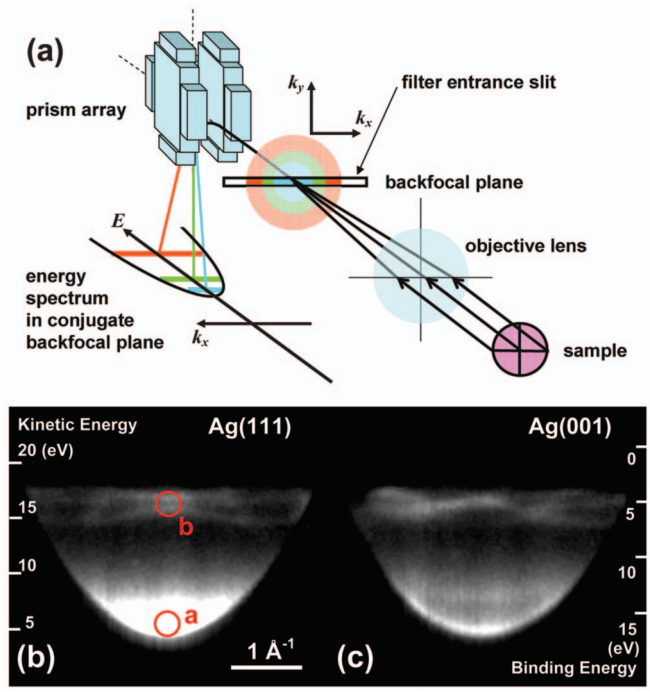

FIG. 1. (Color) (a) Schematics of the LEEM optics equipped with a filter entrance slit in the objective lens back focal plane. Photoelectrons with different energies (red, green, and blue) have corresponding Ewald spheres (shaded disks) in the back focal plane. The position controlled entrance slit selects a slice at a given k_y, which is dispersed by the prism array to form a parabolic energy spectrum image in the conjugate back focal plane. E-k_x spectrum images (signals accumulated for 150 s) from (b) Ag(111) and (c) Ag(001) domains in a single Ag island formed on Si(111) exhibit distinctive differences in the secondary electron intensity at the bottom of parabolas and the fine structure of *d*-band lines, reflecting their electronic structures. The slit is placed nearby the $\bar{\Gamma}$ point. Red circles illustrate the positions of the contrast aperture for the energy-filtered PEEM imaging presented in Fig. 2.

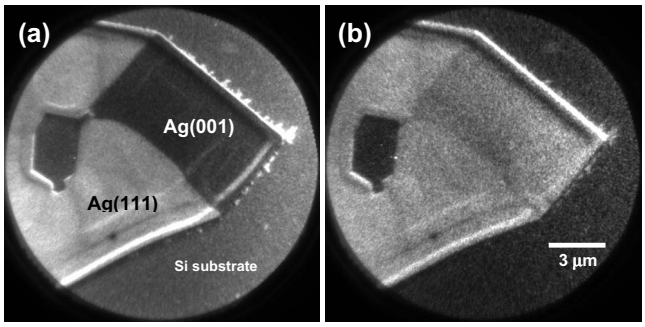

FIG. 2. Energy-filtered PEEM images of a mixed Ag(111)-Ag(001) island with (a) secondary electrons and (b) *d*-band photoelectrons close to the $\bar{\Gamma}$ point (within ± 0.13 Å^{-1}) with a *k*-range width of 0.25 Å^{-1}.

the energy and angular distribution of the photoelectrons can be measured over the full surface Brillouin zone (SBZ). An unpolarized He discharge lamp (Specs UVS300) with focusing capillary and a Hg lamp were installed for PEEM experiments with an incident angle of 70° to the sample surface.

Samples were prepared following the method described in Ref. 11. Ag islands grown on a Si(111) substrate were observed by conventional Hg PEEM, which gives a distinctive contrast between brighter Ag(111) and darker Ag(001) areas.[11] Using an area-selected aperture to limit the observation area to 3.5 μm in diameter, He I photoemission spectra from Ag(111) [Fig. 1(b)] and Ag(001) [Fig. 1(c)] domains are imaged with an energy resolution of 0.16 eV.[11] In these 2D *E*-*k* maps strong *d*-band features can be seen with a dispersion that depends on the surface orientation. Another difference between Ag(111) and Ag(001) spectra can be seen in the secondary electron area. While a high secondary electron intensity with smooth decay toward the *d* band is seen in the case of Ag(111), the Ag(001) spectrum exhibits a significant dip around 2 eV above the vacuum level, near the bottom of the parabola in Fig. 1(c). This dip in the secondary electron intensity corresponds to an absence of final states along the Γ-*X* direction near the vacuum level, as observed previously by normal photoemission and current absorbance spectra.[12] This demonstrates that Hg PEEM contrast is not determined only by work function [which is identical for Ag(111) and Ag(001)] but also by initial- and final-state effects.

By placing a contrast aperture (20 μm in diameter, corresponding to 2.2 eV energy and 0.25 Å^{-1} wave-vector

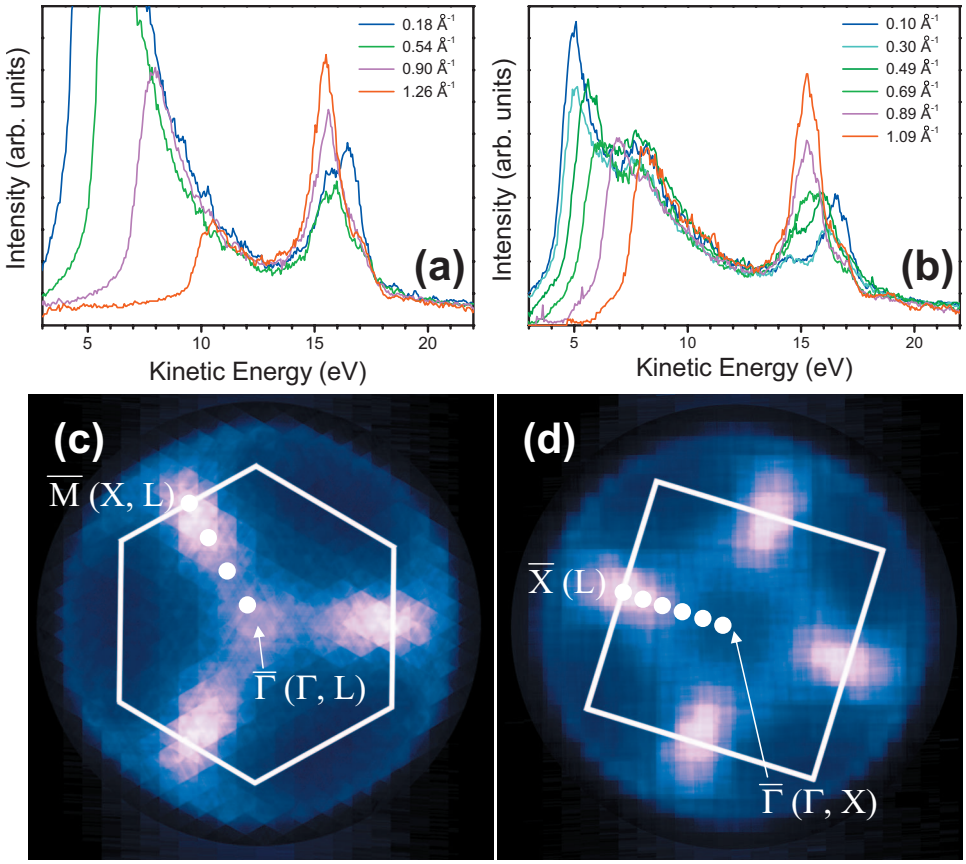

FIG. 3. (Color) Photoemission spectra from (a) $\bar{\Gamma}$-$\bar{M}$ line of Ag(111) and (b) $\bar{\Gamma}$-$\bar{X}$ line from Ag(001) areas, up to the edges of their SBZs. Bulk *L* points have their projections both on the $\bar{\Gamma}$ and the $\bar{M}$ points for Ag(111) and only on the $\bar{X}$ points for Ag(001). Strong resonance is seen at the kinetic energies of ~15.5 eV at each *L* point projections at the SBZ edges, while the resonance is weaker at $\bar{\Gamma}$ on Ag(111). Energy slice images of photoelectrons at the *L* resonance distributed in projection of Ewald sphere on the 2D reciprocal space are reconstructed from 22 *E*-*k* images for (c) Ag(111) and (d) Ag(001) surfaces. The images are symmetrized following the observed symmetries by overlapping the rotated images. White lines represent the SBZ edges. White dots indicate the positions selected for the spectroscopic analyses shown in (a) and (b), and high-symmetry points of the bulk BZ projected onto each of related SBZ points are labeled in the bracket.

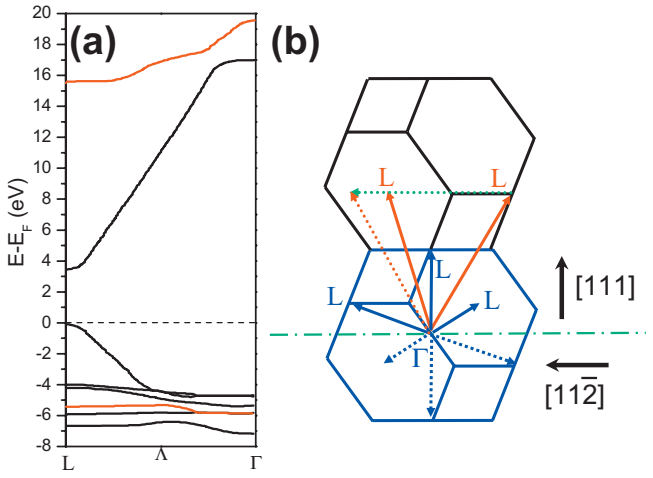

FIG. 4. (Color) (a) Band-structure schematics of Ag along the Λ line after Ref. 18. The valence bands are known to be observed at deeper energies by ~0.3 eV (Ref. 17). Valence and conduction bands related to the strongest *L* resonance are presented by red lines. (b) A schematic sketch of the final states in *L* resonance conditions on Ag(111). Blue lines represent the first BZ, and reduced wave vectors for all *L* points are described by blue arrows. The *L* points (solid red arrows) belonging to the second BZ (black lines) serve as the real momentums for the *L* resonance. Surface scattering (green dotted arrow) effect to produce sixfold component (red dotted arrow) is not observable in the actual photoelectron map [Fig. 3(c)]. Note that it corresponds to a surface reciprocal unit vector that produces $\{\bar{1}0\}$ surface diffraction.

bandwidths[11]) in the energy-filtered back focal plane below the prism [see Fig. 1(b)], energy and wave vector filtered real-space images can be obtained. The secondary electron image [Fig. 2(a)] exhibits significant contrast between brighter Ag(111) and darker Ag(001) domains because of the difference in secondary electron intensity seen in Fig. 1. The Si(111) substrate appears darker than Ag(111) but brighter than Ag(001) in this image. On the other hand, the *d*-band electron image [Fig. 2(b)] gives similar intensity for the two Ag surfaces, while the Si substrate area appears dark, reflecting the fact that there is only 1/3 monolayer of Ag on the Si(111)-$\sqrt{3}\times\sqrt{3}$ substrate. These results indicate that imaging of band distributions (empty state and Ag *d* band) in the Ag islands is readily achieved with a conventional He I discharge lamp, with typical image acquisition times of 5–20 s. The spatial resolution at the boundary between Ag(111) and Ag(001) is measured to be 130 nm, 30 nm wider than the bright field LEEM observation of the same island.[11] This broadening is attributed to the chromatic aberration of the system with wider energy bandwidth and is calculated to be 80 nm, in agreement with the sharpest features observed at the island edge.

In reciprocal space, our experiments reveal the occurrence of sharp resonance peaks in the Ag *d*-band electron energy spectra. Such strong photoemission peaks can be understood by a resonance condition, in which the energy difference between initial and final states just equals the photon energy of the excitation source.[13–17] However, such resonances have only been well studied along normal emission. In order to obtain further understanding of the photoemission process, the position of the filter entrance slit was scanned to obtain successive *E-k* dispersion images to cover the full Ewald sphere. A single scan for 22 *E-k* images was completed within an hour, spending 150 s for an image. Representative energy spectra are shown in Figs. 3(a) and 3(b), for a number of parallel wave vectors along high-symmetry lines between the $\bar{\Gamma}$ points and the edges of the Ag(111) and Ag(001) SBZs, as indicated in Figs. 3(c) and 3(d). Among all *d*-band spectra, the center of the SBZ edges, which coincide with the bulk *L* point projections [$\bar{M}$ for Ag(111) and $\bar{X}$ for Ag(001)], exhibits the strongest resonances for both surfaces at kinetic energies of 15.5 eV (binding energy: 5.7 eV) for Ag(111) and 15.3 eV (binding energy: 5.9 eV) for Ag(001), as seen in Figs. 3(a) and 3(b). These resonances correspond to transitions from L_6^+ (third band) to L_6^- (eighth band) at the bulk *L* point[17] in the theory of Eckardt [Fig. 4(a)],[18] where both initial and final states have flat band structures with a high DOS and band separation of ~21.2 eV, i.e., the energy of the illuminating He I UV line. Another, weaker resonance at a kinetic energy of 16.5 eV (binding energy of 4.7 eV) is observed at the $\bar{\Gamma}$ points of both Ag(111) and Ag(001), which can be roughly understood by the Γ_8^+ (fifth and sixth bands)-Γ_7^- (seventh band) transition. The weaker resonance intensity compared to that of the *L* resonance may be attributed to the slight mismatch between the kinetic energy and the flat band energy at Γ_7^- (17.0 eV). This flat band is known to produce fixed kinetic-energy peaks in normal-emission spectra with higher photon energies.[16,17] The signal intensity from the Ag Fermi-level electrons is known to be very weak in the He I spectrum[13] due to lack of final states for 21.2 eV excitation,[18] and the noise level of our detector, particularly with the very narrow field of view and relatively short acquisition times (150 s/spectrum), was sufficiently high to mask this weak signal. This is not an intrinsic limitation: both *d*-band and Fermi electron maps have been observed using PEEM on Cu(111),[19] where the signal intensity from the Fermi level is much stronger[19] due to matching final states.[18] Energy slices of the photoelectrons in 2D reciprocal space are reconstructed from our dispersion images to visualize the structure of the *d* band, exhibiting prominent threefold and fourfold symmetries for Ag(111) and Ag(001) surfaces, respectively. The representative slices for Ag(111) and Ag(001) surfaces at the strongest *L* resonance are shown in Figs. 3(c) and 3(d) with superimposed SBZs.

The Ag(111) distributions [Fig. 3(c)] show a pronounced lack of sixfold symmetry at the SBZ edges. As seen in Fig. 3(c), while three of the SBZ edges exhibit the strongest resonance, the opposite sides become darkest. While strong resonant emission has previously been observed on the Γ*LUX* plane in ARUPS,[20] the entire absence of the resonance on the opposite side, i.e., the Γ*LKL* plane, has not been previously reported. This observation applies to all *d*-band maps (not shown) observed across a range of energies. Because in principle the surface reciprocal wave vector can transfer the SBZ edge to the opposite side, any phenomena related to the interaction between photoelectrons and the surface periodic potential can result in sixfold symmetry at the hexagonal SBZ edge. Therefore, the lack of such symmetry indicates that the photoemission process of the strongest resonance is

completed without significant influence from the surface periodic potential, implying that the surface potential of Ag(111) is generally transparent for these *d*-band photoelectrons.

The threefold symmetry of the *L* resonance indicates that the unreduced wave vector, with its particular sign and magnitude, is maintained for the final states. Wave-vector selection in the final states has been discussed in detail for transitions nearby the Γ point to the Γ_7^- (seventh) band,[16,17] applying a free-electron model.[20] According to this model, the photon energy of He I used for our experiments should place the final-state wave vectors for the *d*-band excitations in the second BZ rather than in the first BZ.[16] In the case of the *L*-point transitions to the eighth band discussed here, this free-electron model determines the closest *L* points in the second BZ [red solid arrows in Fig. 4(b)] to be the unreduced wave vectors for the final state. These wave vectors belonging to the ΓLUX plane explain the threefold symmetry of our photoemission map.

Energy-filtered photoelectron imaging at the nanoscale and band dispersion imaging at the micrometer scale were achieved on Ag surfaces using a LEEM setup with a highly simplified energy filter. Area-selected band-structure imaging has enabled the comparison of spectra obtained from the full reciprocal space of differently oriented surfaces. The results highlight the importance of the final state in determining the photoemission process and the symmetry of the photoelectron distribution, which is well preserved because of negligible scattering probability of photoelectrons at the Ag(111) surface potential. The potential of this LEEM/PEEM setup, enabling comprehensive photoemission experiments on micrometer scale selected areas using conventional laboratory-based light sources, will open up possibilities in photoemission spectroscopy combined with real-space imaging.

The work by Y.F. was supported by a Grant-in-Aid for Scientific Research from the Japan Society for the Promotion of Science.

[1] F. J. Himpsel, Adv. Phys. **32**, 1 (1983).
[2] E. Bauer, Rep. Prog. Phys. **57**, 895 (1994).
[3] Frank-J. Meyer zu Heringdorf, M. C. Reuter, and R. M. Tromp, Nature (London) **412**, 517 (2001).
[4] A. Kubo, K. Onda, H. Petek, Z. Sun, Y. S. Jung, and H. K. Kim, Nano Lett. **5**, 1123 (2005).
[5] A. Kubo, N. Pontius, and H. Petek, Nano Lett. **7**, 470 (2007).
[6] Frank-J. Meyer zu Heringdorf, Th. Schmidt, S. Heun, R. Hild, P. Zahl, B. Ressel, E. Bauer, and M. Horn-von Hoegen, Phys. Rev. Lett. **86**, 5088 (2001).
[7] Th. Schmidt, J. I. Flege, S. Gangopadhyay, T. Clausen, A. Locatelli, S. Heun, and J. Falta, Phys. Rev. Lett. **98**, 066104 (2007).
[8] F. Nolting, A. Scholl, J. StoÈhr, J. W. Seo, J. Fompeyrine, H. Siegwart, J.-P. Locquet, S. Anders, J. Lüning, E. E. Fullerton, M. F. Toney, M. R. Scheinfeink, and H. A. Padmore, Nature (London) **405**, 767 (2000).
[9] R. M. Tromp, Y. Fujikawa, J. B. Hannon, A. W. Ellis, A. Berghaus, and O. Schaff, J. Phys.: Condens. Matter (to be published).
[10] R. Tromp, M. Mankos, M. Reuter, A. Ellis, and M. Copel, Surf. Rev. Lett. **5**, 1189 (1998).
[11] Y. Fujikawa, T. Sakurai, and R. M. Tromp, Phys. Rev. Lett. **100**, 126803 (2008).
[12] A. Otto and B. Reihl, Phys. Rev. B **41**, 9752 (1990).
[13] H. F. Roloff and H. Neddermeyer, Solid State Commun. **21**, 561 (1977).
[14] R. Courths, H. Wern, U. Hau, B. Cord, V. Bachelier, and S. Hüfner, J. Phys. F: Met. Phys. **14**, 1559 (1984).
[15] E. Tamura, R. Feder, B. Vogt, B. Schmiedeskamp, and U. Heinzmann, Z. Phys. B: Condens. Matter **77**, 129 (1989).
[16] P. S. Wehner, R. S. Williams, S. D. Kevan, D. Denley, and D. A. Shirley, Phys. Rev. B **19**, 6164 (1979).
[17] J. G. Nelson, S. Kim, W. J. Gignac, R. S. Williams, J. G. Tobin, S. W. Robey, and D. A. Shirley, Phys. Rev. B **32**, 3465 (1985).
[18] H. Eckardt, L. Fritsche, and J. Noffke, J. Phys. F: Met. Phys. **14**, 97 (1984).
[19] B. Krömker, M. Escher, D. Funnemann, D. Hartung, H. Engelhard, and J. Kirschner, Rev. Sci. Instrum. **79**, 053702 (2008).
[20] D. Liebowitz and N. J. Shevchik, Phys. Rev. B **17**, 3825 (1978).